

Learning Few-shot Open-set Classifiers using Exemplar Reconstruction

Sayak Nag^{1,*}, Dripta S. Raychaudhuri^{1,*}, Sujoy Paul^{2,†}, Amit K. Roy-Chowdhury¹

¹ University of California, Riverside, ² Google Research
 {snag001@, drayc001@, spaul003@, amitrc@ece.}ucr.edu

Abstract

We study the problem of how to identify samples from unseen categories (open-set classification) when there are only a few samples given from the seen categories (few-shot setting). The challenge of learning a good abstraction for a class with very few samples makes it extremely difficult to detect samples from the unseen categories; consequently, open-set recognition has received minimal attention in the few-shot setting. Most open-set few-shot classification methods regularize the softmax score to indicate uniform probability for open class samples but we argue that this approach is often inaccurate, especially at a fine-grained level. Instead, we propose a novel exemplar reconstruction based meta learning strategy for jointly detecting open class samples, as well as, categorising samples from seen classes via metric based classification. The exemplars, which act as representatives of a class, can either be provided in the training dataset or estimated in the feature domain. Our framework, named Reconstructing Exemplar based Few-shot Open-set Classifier (ReFOCS), is tested on a wide variety of datasets and the experimental results clearly highlight our method as the new state of the art.

1. Introduction

Deep neural networks have achieved excellent performance on a wide variety of visual tasks [9, 19, 23]. However, the majority of this success has been realized under the closed-set scenario, where the training datasets are assumed to include all classes that appear during inference. Real-world applications, on the other hand, often entail acute difficulty in obtaining samples which exhaust all possible semantic categories [22]. This inherent open-ended nature of the visual world restricts the wide-scale applicability of deep models, and machine learning models in general. Thus, it is more realistic to consider an *open-set* scenario, where the predictive model can additionally recognise *out-of-distribution*

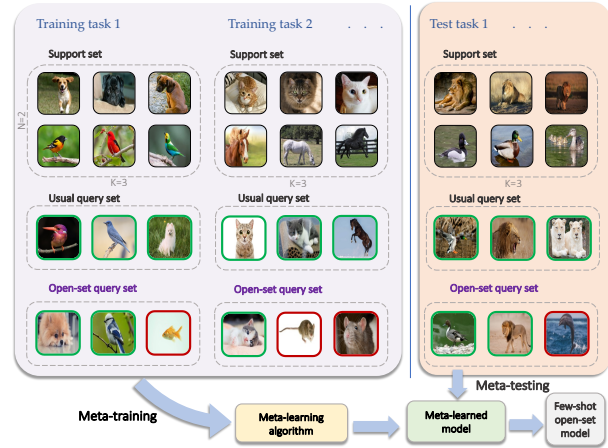


Figure 1: **Problem setup.** We formulate few-shot open-set recognition as a meta-learning problem where training proceeds in an episodic manner. In contrast to the usual setup, where the support and query sets share the same categories, we consider the more challenging open-set scenario where the query set can contain samples from classes not seen in the support (highlighted in red).

samples (not belonging to any of the seen categories), instead of falsely predicting one of the training categories.

Such open-set recognition has been tackled in the literature for the fully supervised setting. Notable approaches involve inducing self-awareness in CNNs [11] to reject out-of-distribution samples, adversarial training [24] to reject adversarial samples which are too hard to classify, and using extreme value statistics to re-calibrate classification scores of samples from novel classes [1]. All of these approaches require large amounts of labeled data per category for the seen classes. On the contrary, humans can easily grasp new concepts with very limited supervision and simultaneously perceive the occurrence of unforeseen abnormalities. Aiming to emulate this, we seek to perform open-set recognition in the few-shot learning scenario, which has been largely ignored in the literature. A visual description of the problem setting is shown in Fig. 1.

The challenge in few-shot open-set recognition stems

*Equal contribution

†Work done while SP was a Ph.D. student at UC Riverside.

from the limited availability of samples for in-distribution classes. This complicates learning a good abstraction of the provided categories to comprehensively distinguish between low-likelihood in-distribution samples and actual out-of-distribution samples. Recently, Liu et. al. [20] attempt this task using Prototypical Networks in a meta-learning setup [5, 37, 32]. Their approach maximizes the entropy over the predicted softmax scores of samples from open classes in an attempt to maximize model confusion for such unseen categories. Thus, out-of-distribution samples are desired to have a uniform predictive distribution. Unfortunately, this assumption does not hold in practice: the sensitivity of deep CNNs to minor perturbations in the input [8], in addition to the softmax function being a smooth variant of the indicator function, make them prone to producing high confidence false predictions for out-of-distribution samples [11]. This is further explained in Fig. 2.

Seeking to rectify this phenomenon, we propose a different approach to detecting out-of-distribution samples in the few-shot setting by utilizing reconstruction as an auxiliary task. Auto-associative networks [27] use a similar concept, with the underlying idea being auto-encoders trained on "normal" data will be able to reconstruct samples from the same distribution but will fail to do so for out-of-distribution instances. However, naively applying reconstruction fails in the few-shot setting due to overfitting. Inspired by [14], we propose to use reconstruction of *class-specific exemplars*, instead of self-reconstruction, to flag out-of-distribution samples. Such exemplars represent the visual category in a canonical domain - devoid of perturbations present in actual real world images - and thus, serve to anchor the representations of in-distribution classes when access to large number of samples is restricted.

Building on this idea of reconstruction, we propose a new meta-learning framework to tackle the few-shot open-set recognition task. In the meta-training phase, we use episodes sampled from a base set, with each episode simulating a token few-shot open-set task. More specifically, each episode is created by randomly selecting a set of classes and populating a support set with limited samples belonging to those classes. A query set is created in a similar fashion, but contains samples from classes both seen in the support set and beyond (see Fig. 1). These episodes are subsequently used to train our proposed framework: Reconstructing Exemplar based Few-shot Open-set ClaSsifer (**ReFOCS**). ReFOCS consists of: (i) a *Reconstruction Module* which aims to reconstruct a sample's corresponding class exemplar, (ii) a *Classification Module* that uses the latent space embedding to perform a metric-based classification of a query sample, and (iii) a *Novelty Detection Module* which utilizes the exemplar reconstruction error, along with the classification score in (ii) and modulated latent space embedding, to recognize the probability of the sample being out-of-distribution.

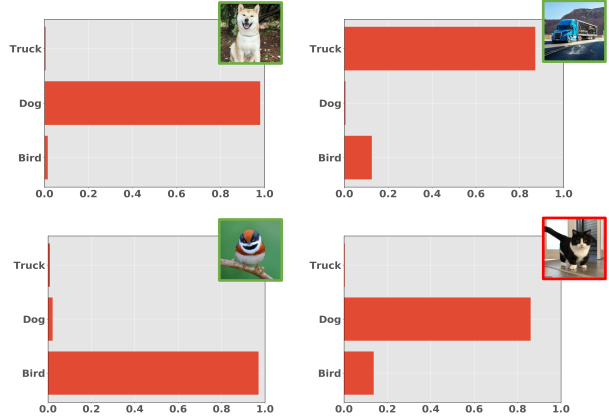


Figure 2: **Assuming uniform predictive distribution for outliers.** Out-of-distribution samples can be correlated to in-distribution classes by varying amounts. In this figure, we train a classifier for three in-distribution classes: dog, bird and truck (corresponding samples highlighted in green). The out-of-distribution sample - a cat - shares highly similar visual characteristics to a dog, as evidenced by the prediction. This suggests that desiring outliers to have a uniform predictive distribution, as suggested in [20], is often inaccurate.

Note that the class-specific exemplars used in the proposed method need not be always provided as images, as we show later that these can also be learnt in the feature space.

Main contributions. Our primary contributions are summarized below:

- We develop a new meta-learning framework which utilizes class-specific exemplars to jointly perform few-shot classification and out-of-distribution detection.
- Aiming to make the learnt representations more robust and discriminative in the presence of scarce samples, we introduce a novel embedding modulation scheme. A weighted strategy for prototype computation is also introduced for reducing intra-class bias.
- In comparison to the current state-of-the art we obtain a median increase of approximately 6% in AUROC for 5-shot experiments and around 7% for 1-shot experiments with a maximum increase of over 12%. The increased AUROC is complemented with greater or comparable classification accuracy of in-distribution samples which altogether clearly establishes our proposed approach as the new state-of-the art in few-shot open-set recognition.

2. Related works

Few-shot learning. Few-shot learning [29, 28] aims to learn representations that generalize well to novel classes with few examples. Meta-learning [12] is the one of the most common approaches for addressing this problem and it is generally grouped into one of the following categories: *gradient-based*

methods [5, 26] and metric learning methods [37, 32]. Typical gradient based methods, such as MAML [5] and Reptile [26], aim to learn a good representation that enables fast adaptation to a new task. On the other hand, metric-based techniques like Matching Networks [37] and Prototypical Networks [32] learn a task-specific kernel function to perform classification via a weighted nearest neighbor scheme. Our framework belongs to the latter class of methods, with the ability to work in the open-set scenario.

Open-set classification. Open-set classification extends the standard classification task by additionally focusing on rejecting samples from unseen classes. Hendrycks et. al. [11] showed that softmax alone is not a good indicator of out-of-distribution probability but statistics drawn from softmax can be utilized to make assumptions of the "normalcy" of a test sample. Liang et. al. [18] re-calibrated output probabilities by applying temperature scaling and used virtual adversarial perturbations to the input to enhance the out-of-distribution capability of the model. Recently, Bendale et. al. [1] introduced OpenMax which uses extreme value statistics to re-calibrate the softmax scores of samples from unseen classes. G-OpenMax [6] combines OpenMax with a generative model to synthesize the distribution of all unseen classes. Recently, counterfactual image generation [25] has been proposed to generate hard samples in an effort to build a more robust model. Note that all these methods are in a fully supervised learning setting and are not directly applicable to few-shot learning. Liu et. al. [20] utilize meta-learning to tackle this problem. Their framework, titled PEELER, builds on top of prototypical networks [32] and uses only softmax scores to detect unseen categories, via maximizing the entropy for the unseen samples while training. Unlike the prior works used in the fully supervised setting [27, 1, 25], PEELER does not try to learn the class cluster of all open classes by clubbing them as a single unseen class, but instead learns the cluster of the seen classes and detects unseen class samples if they do not fall in any of those clusters.

3. Methodology

In this section, we present our framework for open-set few-shot classification. We first provide a definition of the problem, followed by a brief overall methodology, and then present a detailed description of our framework.

Problem Setting. Consider the standard few-shot learning setting, where we have access to a support set of labeled examples $\mathbb{S} = \{S_1, \dots, S_N\}$, with each $S_c = \{\mathbf{x}_i\}_{i=1}^K$ denoting a set of K examples in the support set for K -shot recognition. All of the samples in S_c belong to the class y_c . We also consider that we may be given a canonical exemplar \mathbf{t}_c for every category. Note, as we will discuss subsequently, \mathbf{t}_c can also be estimated instead of being provided with the training set, and we show results for both cases. Unlike the standard few-shot setting, the query set \mathbb{Q} is comprised

of both in-distribution and out-of-distribution samples w.r.t \mathbb{S} , i.e., $\mathbb{Q} = \mathbb{Q}_{in} \cup \mathbb{Q}_{out}$. In-distribution samples belong to classes seen in the support set while out-of-distribution samples belong to unseen classes. The goal is to detect the samples in \mathbb{Q}_{out} as out-of-distribution, while correctly classifying the samples in \mathbb{Q}_{in} .

Similar to the standard few-shot learning setup, we utilize a base set of labeled samples to meta-learn our framework, which can then be used for the few-shot tasks during inference. More specifically, given a labeled base set $\mathcal{B} = \{(\mathbf{x}_i, y_i, \mathbf{t}_i)\}_{i=1}^M$, we construct training episodes by sampling N classes, with support sets comprising of K randomly chosen samples (and corresponding exemplar) belonging to each of the selected classes. A query set is also constructed in a similar fashion. In order to simulate the presence of out-of-distribution samples, we follow the strategy outlined in [20] and augment the query set with samples from classes *absent* in the support.

Overall Framework. A pictorial description of our framework is shown in Fig. 3. Given a sample \mathbf{x} , we first feed it to the reconstruction module. This module returns an embedding of the sample, along with a reconstruction of the possible exemplar \mathbf{t} associated with the ground-truth class of \mathbf{x} . The embedding is used to obtain a classification score, similar to [2, 37], while the reconstructed exemplar is used as a proxy for the out-of-distribution detection task. Specifically, if $\mathbf{x} \in \mathbb{Q}_{out}$, we hypothesize that the decoder of the reconstruction module will fail to reconstruct any of the exemplars of the support classes. The learned embedding, classification scores, and the reconstruction errors, with respect to support exemplars, are then fed into a novelty detection module, which predicts the probability of the sample \mathbf{x} being out-of-distribution.

3.1. Reconstruction Module

The reconstruction module has a two-fold objective: given an input sample \mathbf{x} , learn a latent representation \mathbf{z} which will be used to classify the sample and, secondly, utilize the same representation to reconstruct its corresponding class-specific exemplar image \mathbf{t} via the decoder. The class-specific exemplars \mathbf{t} form a compact representation of the real world images belonging to that class and we hypothesize that the ability to reconstruct any exemplar belonging to in-distribution classes correlates positively with the sample being an in-distribution one. Inspired by [14], we construct this module using a Variational Auto-Encoder (VAE) [16]. The choice of VAE is motivated by its robustness to outliers and better generalization to unseen data, as shown in [3]. This is ideal for the image-to-exemplar translation task where the exemplars lie on a canonical domain devoid of the perturbations in real images.

Given an input sample \mathbf{x} , its exemplar reconstruction of \mathbf{t} is carried out by maximizing the variational lower bound of

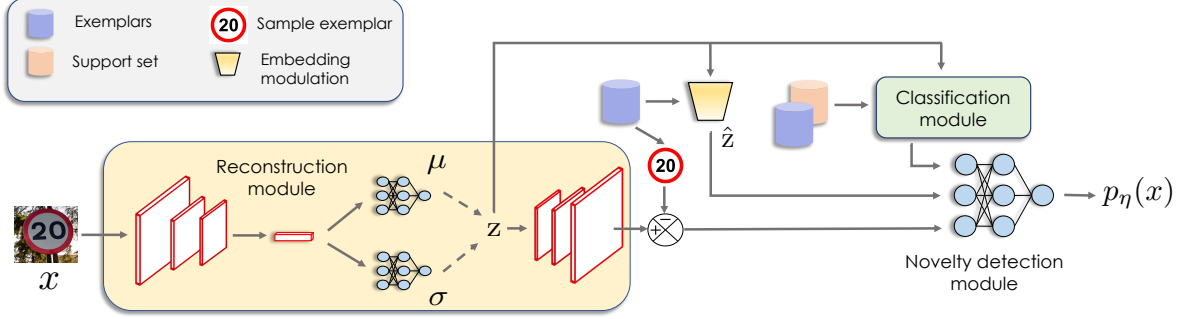


Figure 3: **Overview of framework.** Given a query sample \mathbf{x} , a latent representation \mathbf{z} is derived by sampling from the variational posterior. This embedding is further enhanced via a modulation process to get $\hat{\mathbf{z}}$. The latent embedding and its enhanced version are used for classifying the sample into one of the few-shot classes and also to predict whether it is an out-of-distribution instance by utilizing exemplar reconstruction.

the likelihood $p(\mathbf{t})$ [14] as follows,

$$\log p(\mathbf{t}) \geq \mathbb{E}_{q_\phi(\mathbf{z}|\mathbf{x})}[\log p_\theta(\mathbf{t}|\mathbf{z})] - D_{KL}[q_\phi(\mathbf{z}|\mathbf{x})||p(\mathbf{z})] \quad (1)$$

where $D_{KL}[\cdot]$ is the Kullback-Leibler (KL) divergence and $q_\phi(\mathbf{z}|\mathbf{x})$ denotes the variational distribution introduced to approximate the intractable posterior. Note that this is different from a vanilla VAE [16], which is derived by maximizing the log-likelihood of the input data \mathbf{x} . A differentiable version of the lower bound is derived by assuming the latent variable \mathbf{z} to be Gaussian in nature, sampled from the prior $q_\phi(\mathbf{z}|\mathbf{x})$. The empirical loss to be minimized is given as follows,

$$\mathcal{L}_{VAE} = \frac{1}{K_e} \sum_{i=1}^{K_e} -\log p_\theta(\mathbf{t}_i|\mathbf{z}_i) + D_{KL}[q_\phi(\mathbf{z}|\mathbf{x})||p(\mathbf{z})] \quad (2)$$

where K_e is the number of samples in one episode, i.e., $K_e = |\mathbb{S} \cup \mathbb{Q}_{in}|$. Since $\mathbf{z} \sim q_\phi(\mathbf{z}|\mathbf{x})$ is non-differentiable, the re-parameterization trick is applied via the decoder network [16] such that $\mathbf{z} = \mu + \sigma \odot \epsilon$, where $\epsilon \sim \mathcal{N}(0, \mathbf{I})$ and \odot is the Hadamard product.

The first term in Eq. 2 is the reconstruction loss which affects the mapping of the real images to their class specific exemplars, while the second term acts as a distribution regularization enforcing \mathbf{z} to follow the chosen prior. Although binary cross entropy (BCE) is the common choice for the reconstruction loss in VAE, other losses such as l_1 or l_2 norm can also be used. The type of reconstruction loss used in each of our experiments can be found in Section 4.

3.2. Classification Module

As discussed in Section 3.1, the embedding \mathbf{z}_q , of a query sample \mathbf{x}_q , is also used for obtaining the classification scores. This is done by computing a softmax over the logits obtained from computing the cosine similarity between \mathbf{z}_q and the set of prototypes or centroids, $\{\Omega_c\}_{c=1}^N$ for each class $c \in \mathbb{S}$ (Fig. 3). In contrast to prior works [32, 20], the class specific

prototype Ω_c is obtained by a weighted mean of the support samples instead of a simple mean. Note that these prototypes are different from the class specific exemplars \mathbf{t} .

Prototype computation. Given the support set, the prototypes for each class c are calculated as follows,

$$\Omega_c = \frac{1}{K} \sum_{k=1}^K \omega_k \cdot \mathbf{z}_k^c \quad (3)$$

\mathbf{z}_k^c denotes the latent representation of $\mathbf{x}^k \in \mathbb{S}_c$, while ω_k is the weight assigned to \mathbf{z}_k^c based on how close it is from the embedding of the exemplar belonging to the c^{th} class, \mathbf{z}_t^c ,

$$\omega_k = \frac{e^{\cos(\mathbf{z}_k^c, \mathbf{z}_t^c)}}{\sum_{k=1}^K e^{\cos(\mathbf{z}_k^c, \mathbf{z}_t^c)}} \quad (4)$$

We use these weights in an effort to control the phenomena of *intra-class bias* [21], i.e., the difference between the true expected prototype and the Monte-Carlo estimated value. As explained earlier, the exemplars, which lie on a canonical domain, provide an effective ideogram of the images in the real domain and the embedding of the real images cluster around their corresponding exemplars. Thus, the exemplars are a good approximation of the true prototype and we leverage this via the weights ω_k to alleviate the intra-class bias.

Classification. After computing the prototypes, we predict the classification scores for the query sample x_q as follows,

$$p_\phi(y = c|\mathbf{x}_q) = \frac{e^{\tau \cdot \cos(\mathbf{z}_q, \Omega_c)}}{\sum_{c'} e^{\tau \cdot \cos(\mathbf{z}_q, \Omega_{c'})}} \quad (5)$$

where τ is a learnable temperature parameter to scale the logits computed by cosine similarity [2, 7]. Learning proceeds by minimizing a cross-entropy loss over the in-distribution classes as follows:

$$\mathcal{L}_{CE} = -\frac{1}{|\mathbb{Q}_{in}|} \sum_{i=1}^{|\mathbb{Q}_{in}|} \sum_{c=1}^N \mathbb{1}\{y_i = c\} \log p_\phi(y = c | \mathbf{x}_{q,i}) \quad (6)$$

where y_i represents the true class of the query sample.

3.3. Novelty detection Module

The novelty detection module models the probability of a data point being an out-of-distribution sample. It takes in three different sources of information as input: (i) the class probability \mathbf{p}_ϕ as predicted by the classification module in Eq. 5, (ii) a modulated version of the embedding \mathbf{z} (described below), and (iii) the vector of reconstruction errors with respect to the support set exemplars, $\mathbf{D} = [||\hat{\mathbf{t}} - \mathbf{t}_1||_F^2, \dots, ||\hat{\mathbf{t}} - \mathbf{t}_N||_F^2]$. \mathbf{D} indicates how far the reconstructed exemplar $\hat{\mathbf{t}}$ deviates from the actual exemplar $\mathbf{t} \in \mathbb{S}$. Intuitively, for out-of-distribution samples all the entries of \mathbf{D} will be very high, while for in-distribution samples, at least one of them will be very small.

Embedding Modulation. At a fine-grained level, samples from the seen classes with similar feature representations as in-distribution samples can lead to high confidence false predictions by the softmax operator [11]. Thus, it is vital to obtain an embedding that is discriminative enough to provide good segregation between in-distribution and out-of-distribution samples in the feature space. To enhance the discriminative property of the latent space embedding, we scale the embedding of a query sample \mathbf{z}_q with a scalar $\gamma > 0$ as shown below,

$$\hat{\mathbf{z}}_q = \frac{\mathbf{z}_q}{\gamma}, \quad \text{where } \gamma = \min_{c \in \mathbb{S}} ||\mathbf{z}_q - \Omega_c||_1 \quad (7)$$

where $c \in \{1, \dots, N\}$ represents the classes in the support and Ω_c is the prototype corresponding to the c^{th} class. γ measures the "reachability" of \mathbf{z}_q to the in-distribution class centroids or prototypes [31, 22]. Since the samples belonging to a specific class tend to cluster around the embedding of the exemplar, out-of-distribution samples will have a higher value for γ compared to in-distribution samples. This in-turn amplifies the embedding value for the in-distribution queries and scales it down for out-of-distribution queries.

Considering the input to the novelty detection module is a concatenated vector $[\mathbf{p}_\phi, \hat{\mathbf{z}}_q, \mathbf{D}]$, we use an MLP to predict its probability p_η of being from out-of-distribution. The module is trained using binary cross-entropy loss as follows,

$$\mathcal{L}_{BCE} = -\frac{1}{|\mathbb{Q}|} \sum_{i=1}^{|\mathbb{Q}|} y_{\eta,i} \log p_{\eta,i} + (1 - y_{\eta,i}) \log(1 - p_{\eta,i}) \quad (8)$$

where y_η is equal to 0 or 1 depending on whether $x_q \in \mathbb{Q}_{in}$ or $x_q \in \mathbb{Q}_{out}$ respectively.

3.4. Training

The parameters of the Encoder (ϕ), Decoder (θ) and the Novelty module (η) are jointly meta-trained by optimizing over the aggregate loss \mathcal{L} ,

$$\mathcal{L} = \lambda_1 \mathcal{L}_{VAE} + \lambda_2 \mathcal{L}_{CE} + \lambda_3 \mathcal{L}_{BCE} \quad (9)$$

where λ_1 , λ_2 and λ_3 are hyper-parameters, choices of which is discussed in Section 4.

Training without given exemplars. The class-specific exemplars used in our framework need not be always provided as images. In that case, we pass the category wise samples through a ResNet-18 model pre-trained on ImageNet [4] and extract the features from the penultimate fully-connected layer. We then compute the centroid of each class in the feature-space and choose the image whose representation is closest to it as the exemplar of that class.

Testing without given exemplars. In case we do not have exemplars in the test set, we estimate it directly from the support set. We pass the support examples through the encoder to obtain their latent space embedding and compute their mean embedding. We then choose the support sample closest to this centroid as the exemplar of that class and the rest of the process remains the same. In case of 1-shot recognition we use the support sample itself as the exemplar.

4. Experiments

The goal of our evaluation is to answer the following question: *can the proposed framework detect out-of-distribution samples in the few-shot setting in conjunction to correctly classifying the in-distribution samples?* We answer this question in the affirmative through comprehensive experiments over several data sets, which establish our method as the clear state-of-the-art.

Datasets. We use six datasets to setup three different types of open-set recognition tasks: (i) *traffic sign recognition*, for which we use the GTSRB [33] and TT100K [38] datasets, (ii) *brand logo recognition*, for which we use BelgaLogos [13, 17], FlickrLogos-32 [30] and TopLogo-10 [34], and (iii) *natural image classification* on the *miniImageNet* dataset, using the same splits as introduced by Vinyals et.al. [37]. Following [14], the above mentioned datasets are used to configure five few-shot scenarios as shown in Tables 1 and 2. These scenarios are configured by varying the meta-training and meta-testing datasets - such a cross dataset evaluation is more challenging compared to using splits from the same dataset [35]. For the traffic sign and natural image datasets, we evaluate our model on both the 5-way 5-shot and the 5-way 1-shot tasks, while for the logo classification task, we show results only on the 5-way 1-shot scenario. This is due to BelgaLogos and Toplogos having multiple classes with less than 5 samples. More details on these datasets and splits can be found in the supplementary material.

MODEL	METRIC	DATASETS					
		GTSRB→GTSRB		GTSRB→TT100K		miniImageNet→miniImageNet	
		ACC. (%)	AUROC(%)	ACC. (%)	AUROC (%)	ACC. (%)	AUROC (%)
5-way 5-shot							
PROTONET [32]	Euclidean	91.79 ± 0.44	70.74 ± 0.79	80.51 ± 0.78	62.10 ± 0.76	78.11 ± 1.22	58.67 ± 0.45
PROTO+OM [1]	Euclidean	91.92 ± 0.43	86.67 ± 0.48	64.40 ± 0.78	68.80 ± 0.66	79.01 ± 1.21	54.16 ± 0.47
PEELER [20]	Mahalanobis	93.87 ± 0.37	90.99 ± 0.44	79.04 ± 0.79	73.25 ± 0.81	63.60 ± 0.67	64.17 ± 0.64
PEELER ⁺ [20]	Mahalanobis	-	-	-	-	75.08 ± 0.72	69.85 ± 0.70
REFOCS(Ours)	Cosine	94.17 ± 0.38	94.83 ± 0.35	83.36 ± 0.76	85.25 ± 0.56	79.06 ± 1.17	69.91 ± 0.51
5-way 1-shot							
PROTONET [32]	Euclidean	82.31 ± 0.75	61.52 ± 0.90	69.82 ± 0.87	56.02 ± 0.83	51.18 ± 1.36	56.51 ± 0.47
PROTO+OM [1]	Euclidean	82.46 ± 0.70	81.43 ± 0.65	55.10 ± 0.80	67.79 ± 0.66	51.13 ± 1.36	45.09 ± 0.39
PEELER [20]	Mahalanobis	82.86 ± 0.77	79.56 ± 0.85	73.47 ± 0.88	69.68 ± 0.88	48.49 ± 0.81	59.39 ± 0.77
PEELER ⁺ [20]	Mahalanobis	-	-	-	-	58.31 ± 0.58	61.66 ± 0.62
REFOCS (Ours)	Cosine	86.21 ± 0.78	93.02 ± 0.45	71.45 ± 0.87	81.98 ± 0.59	51.48 ± 1.19	67.49 ± 0.59

Table 1: **5-way 5-shot and 5-way 1-shot results of traffic sign and natural image classification.** For both traffic sign datasets GTSRB→GTSRB and GTSRB→TT100K, 800 test episodes were evaluated and the average performance is reported. For the natural images the performance is averaged over 600 test episodes. PEELER⁺ denotes the corresponding results reported in [20] while PEELER, in the previous row, denotes the results obtained via the official implementation². All results are reported with 95% confidence levels.

Implementation. For the traffic sign and logo classification experiments, the VAE architecture is adapted from [14], while for the natural image classification task, we design the VAE using a ResNet-18 [10] encoder and an inverted ResNet-18¹ as the decoder. The novelty module is implemented as a multi-layered perceptron with two hidden layers of 200 and 100 nodes respectively. For a fair comparison, the encoder network is kept the same for all competing methods. Similar to [14], the embedding size is set to 300 for the traffic sign and logo datasets, while the ResNet-18 encoder is used to obtain a 2048 dimensional feature representation for the natural image classification task. The Adam optimizer [15] is used for all the experiments. The choice of hyperparameters for each experiment along with their individual episodic sampling strategies are described in the supplementary material.

Baselines. We compare ReFOCS against Prototypical Networks (ProtoNet) [32], which is implemented with the euclidean distance metric, and PEELER [20] which uses the Mahalanobis distance metric. While not originally designed for open-set classification, ProtoNet provides a lower bound on performance for comparison, and on the other hand, PEELER is the sole method, to the best of our knowledge, that addresses few-shot open-set classification. We also compare against OpenMax [1], which was originally proposed for out-of-distribution detection in the fully supervised setting. Since OpenMax re-calibrates the softmax score to reject out-of-distribution samples, we implement it over the

standard prototypical network in order to adapt it for the few-shot setting, and henceforth we denote this as Proto+OM.

Evaluation Metrics. To quantify the closed-set classification performance we compute the accuracy over in-distribution queries, and utilize the Area Under the Receiver Operating Characteristic curve (AUROC) to quantify the model’s performance in detecting the open classes. For all our evaluations, we split the query set equally among in-distribution and out-of-distribution samples.

4.1. Traffic Sign Recognition

The performance of ReFOCS on the two traffic sign recognition tasks, GTSRB→GTSRB and GTSRB→TT100K, is shown in Table 1. For both cases, the framework was meta-trained for 20000 episodes and the standard BCE criterion was used for computing the VAE reconstruction loss. As shown in Table 1, ReFOCS outperforms all baselines in detecting the out-of-distribution samples. On average, the AUROC score achieved by ReFOCS is 10.4% higher than the competing methods. The problem of using softmax values as an open-set indicator can be clearly seen in the lower AUROC values of ProtoNet, Proto+OM and PEELER. The issue is more pronounced for ProtoNet, since, unlike the PEELER and Proto+OM, ProtoNet does not explicitly regularize the probability scores of out-of-distribution samples which results in even more high-confidence false predictions. The efficacy of our proposed prototype computation (Eq. 4) is also evidenced by the higher classification accuracy - 1.22% on average - in comparison to the baselines. This shows that the weighted prototype computation leads

¹<https://github.com/julianstastny/VAE-ResNet18-PyTorch>

to more *unbiased* prototypes as opposed to those computed baselines.

4.2. Brand Logo Recognition

The brand logo datasets consist of everyday images of commercial brand logos. In both of the two few-shot tasks, Belga→Flickr32, and Belga→Toplogos, the Belga dataset is used for meta-training our framework. Since some of the classes have as low as 2 samples, we restrict our experiments to the 5-way 1-shot scenario (Table 2). We meta-train our framework for 50000 episodes these tasks. From the results shown in Table 2, it is evident that ReFOCS achieves significant gains in both accuracy and AUROC, outperforming PEELER [20] by an average of 4.28% in AUROC and 3.05% in classification accuracy. This clearly highlights the superiority of our approach for few-shot open-set recognition. The in-distribution classification accuracy, although better than the competing baselines, is lower in comparison to the traffic sign datasets, which is due to the lower quality of the training set, as pointed out in [14]. In addition, there is a significant domain gap between the images and exemplars of Belga and that of Toplogos, which makes it even more difficult to achieve good classification accuracy.

MODEL	METRIC	BELGA→FLICKR32	
		ACC. (%)	AUROC(%)
PROTONET [32]	Euclidean	59.50 ± 0.99	58.69 ± 0.94
PROTO+OM [1]	Euclidean	59.60 ± 1.01	61.00 ± 1.02
PEELER [20]	Mahalanobis	62.93 ± 1.03	66.40 ± 0.86
REFOCS (Ours)	Cosine	66.29 ± 1.02	72.98 ± 0.83
BELGA→TOPLOGOS			
		ACC. (%)	AUROC(%)
PROTONET [32]	Euclidean	38.08 ± 2.10	53.18 ± 1.97
OPENMAX [1]	Euclidean	38.20 ± 1.95	56.40 ± 1.92
PEELER [20]	Mahalanobis	39.55 ± 2.05	56.25 ± 1.94
REFOCS (Ours)	Cosine	42.30 ± 2.15	58.39 ± 1.97

Table 2: **5-way 1-shot results of brand logo recognition.** For **Belga→Flickr32**, 1700 test episodes were evaluated and for **Belga→Toplogos**, 400 test episodes were evaluated and their average closed-set Accuracy and open-set AUROC are reported with 95% confidence intervals.

4.3. Natural Image Classification

miniImageNet is not explicitly provided with categorical exemplars and thus, we use the strategy explained in Section 3.4 to estimate the exemplars in our framework. For both the 5-way 5-shot and 5-way 1-shot scenarios, ReFOCS is meta-trained with 50000 episodes. It must be noted that the chosen exemplars are not on a canonical domain unlike those of the traffic sign and brand logo datasets. This makes the image-to-image translation for exemplar reconstruction even more challenging, specifically due to the presence of varying lighting and color contrasts in the real domain. Con-

sequently, the standard BCE reconstruction loss is not able to compensate for these perturbations, and thus, we use the ℓ_2 norm as the reconstruction criterion, which leads to a marked improvement in the results. From Table 1 we can clearly see that ReFOCS outperforms the baselines especially for the open sample detection as evidenced by the higher AUROC scores. Many of the *miniImageNet* objects have fine-grained visual differences (eg: cats and dogs) - this makes ProtoNet, which relies on the raw softmax score, prone to misclassification of the unseen categories as one of the seen ones. This is reflected in the performance of ProtoNet as it is barely able to achieve better than random AUROC (Table 1). Unlike the prior experiments, Proto+OM fails to achieve a decent AUROC score. This is predominantly due to the failure of OpenMax to fit a Weibull distribution with few samples for a dataset of natural images like *miniImageNet* which is more complex compared to the traffic sign and logo datasets. As a result, OpenMax fails to recalibrate the ProtoNet’s logits with such few number of support samples. Note that PEELER fails to achieve the reported performance on the *miniImageNet* experiments [20] when results are generated by using the official implementation ².

4.4. Ablation Studies

In this section we use two cross-dataset scenarios to perform ablation studies of different components of our framework to understand their contribution towards the final performance.

Impact of using variational encoding. The reconstruction module of ReFOCS is designed using a VAE [14] due to its better generalization ability [3]. We highlight this by replacing the VAE and experimenting with a standard auto-encoder (AE). As shown in Table 3, the classification performance drops significantly, along with a drop in the AUROC.

Impact of embedding modulation. The importance of the embedding modulation can be clearly seen from Table 3. The modulated embedding results in more distinct feature representations with adequate segregation between the seen and unseen classes, thereby, making it easier for the novelty module to flag unseen categories. Removing it results in a significant drop in AUROC and on the other hand it’s presence also amplifies the classification performance. This suggests that the improvement of the open class detection is complemented by improvement in seen class categorisation.

Input to the novelty module. We feed a concatenation of the modulated embedding, classification score and ℓ_2 reconstruction errors to the novelty module. Empirically, the combination of all three gives the best results for out-of-distribution detection. We study the impact of removing the classification score or the embedding from the input and as seen from the results in Table 3, in both cases there is a drop in both the classification accuracy and the AUROC score.

²<https://github.com/BoLiu-SVCL/meta-open/>

EXPERIMENT	GTSRB→TT100K		BELGA→FLICKR32	
	5-way 5-shot		5-way 1-shot	
	Acc.(%)	AUROC(%)	Acc.(%)	AUROC(%)
Recons. w/ AE	81.33 ± 0.80	77.08 ± 0.79	63.13 ± 1.05	71.86 ± 0.86
No modulation	80.94 ± 0.79	78.55 ± 0.65	63.26 ± 1.03	56.69 ± 0.97
ProtoC+ND	76.92 ± 0.83	72.50 ± 0.61	61.64 ± 1.03	50.01 ± 0.99
No embedding	83.03 ± 0.75	74.33 ± 0.66	65.49 ± 1.00	67.79 ± 0.91
No clf	82.71 ± 0.74	82.85 ± 0.56	64.51 ± 1.01	71.58 ± 0.87
ReFOCS (Ours)	83.36 ± 0.76	85.25 ± 0.56	66.29 ± 1.02	72.98 ± 0.83

Table 3: **Ablation studies.** Recons. w/ AE refers to swapping the VAE with an Autoencoder (AE); No Modulation denotes turning off embedding modulation; No embedding/clf denote the removal of embedding/softmax scores from the input of the novelty module. ProtoC+ND refers to when we do not use exemplars for the reconstruction and consequently, remove the reconstruction errors from the input of the novelty module.

DATASET	SETTING	METRIC	Acc.	AUROC
GTSRB→TT100K	5-shot	Cosine	83.36 ± 0.76	85.25 ± 0.56
		Euclidean	78.77 ± 0.74	81.42 ± 0.51
Belga→Flickr32	1-shot	Cosine	66.2 ± 1.02	72.9 ± 0.83
		Euclidean	48.73 ± 0.99	50.61 ± 0.95
miniImagenet	5-shot	Cosine	79.06 ± 1.17	69.91 ± 0.51
		Euclidean	79.09 ± 1.15	52.83 ± 0.48

Table 4: **Choice of metric.** Effect on performance as the similarity metric is varied.

Additionally, we also examine the scenario when we do not use any exemplar for reconstruction, and consequently, feed in just the classification score and the raw embedding as input to the novelty module. We call this variant of ReFOCS, ProtoC+ND and as seen from Table 3 the removal of the exemplar reconstruction errors result in the biggest drop in performance - with AUROC dropping to 50% in one case (random prediction) - which again consolidates the impact of the exemplars in out-of-distribution detection.

Choice of distance metric. Computing the logits for classification requires a distance metric to measure the similarity between the prototypes and the sample in the latent space. We experiment with both the cosine and euclidean metrics and choose the cosine distance as it leads to more a discriminative embedding space [7, 21]. This is particularly important for segregating the open class samples from the support class ones. This is validated by the results shown in Table 4, where we can see that choosing the euclidean distance metric leads to a significant drop in AUROC.

Varying hyperparameters. Fig. 4 shows an how the open-

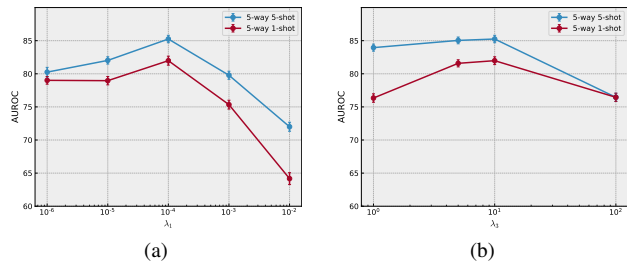


Figure 4: **Hyperparameter Analysis.** (a) λ_2 & λ_3 are fixed at 5 and 10, changing only the reconstruction loss term. (b) λ_1 and λ_2 are fixed at 10^{-4} and 10 and λ_3 is varied.

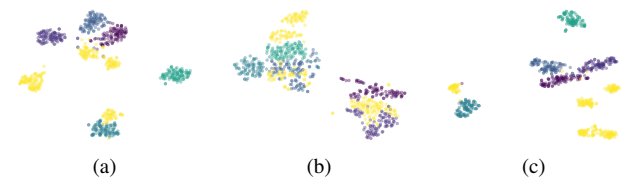


Figure 5: **t-SNE visualization.** We project the latent space learned via (a) ProtoNet (b) PEELER (c) ReFOCS, on 5 classes of GTSRB→TT100K, on a 2D space using t-SNE. Out-of-distribution queries are in yellow

set AUROC is affected by the hyperparameters λ_1 or λ_3 (from Eq. 9) for the GTSRB→TT100K task. In both cases, the classification term λ_2 is fixed at 10. In Fig. 4a, when λ_1 is very low, the open-set detection is hampered due to poor quality of the reconstruction and when it is increased beyond 10^{-4} reconstruction becomes the sole objective of the model, thus the open-set detection again degrades. From Fig. 4b we can see that for both the 5-shot and 1-shot cases increasing λ_3 causes the AUROC to improve the knee point of $\lambda_3 = 10$, after which it starts to degrade.

Embedding Visualization. In Fig. 5 we compare the t-SNE [36] visualization of the embedding spaces induced by all the competing methods. We can see from Fig. 5 that, in general, ReFOCS achieves more distinct class clusters in comparison to both PEELER [20] and ProtoNet [32], with adequate segregation between seen and unseen classes.

5. Conclusion

In this work, we present a novel strategy for addressing few shot open-set recognition. We frame the few-shot open-set classification task as a meta learning problem similar to [20], but unlike their strategy, we do not solely rely on the softmax score as an indication of an open class. We argue that the proclivity of softmax to overfit to unseen classes makes it an unreliable choice as an open-set indicator, especially when there is a dearth of samples. Instead we propose to use a reconstruction of exemplar images as a key

signal to detect out-of-distribution samples. The enhanced performance of our framework is verified empirically over a wide variety of few-shot tasks and the results establish it as the new state-of-the-art. In the future, we would like to extend this approach to more cross-domain few-shot tasks, including videos.

References

- [1] Abhijit Bendale and Terrance E. Boult. Towards open set deep networks. In *Proceedings of the IEEE Conference on Computer Vision and Pattern Recognition (CVPR)*, June 2016. [1](#), [3](#), [6](#), [7](#)
- [2] Yinbo Chen, Xiaolong Wang, Zhuang Liu, Huijuan Xu, and Trevor Darrell. A new meta-baseline for few-shot learning. *arXiv preprint arXiv:2003.04390*, 2020. [3](#), [4](#)
- [3] Bin Dai, Yu Wang, John Aston, Gang Hua, and David Wipf. Connections with robust pca and the role of emergent sparsity in variational autoencoder models. *The Journal of Machine Learning Research*, 19(1):1573–1614, 2018. [3](#), [7](#)
- [4] J. Deng, W. Dong, R. Socher, L. Li, Kai Li, and Li Fei-Fei. Imagenet: A large-scale hierarchical image database. In *2009 IEEE Conference on Computer Vision and Pattern Recognition*, pages 248–255, 2009. [5](#), [11](#)
- [5] Chelsea Finn, Pieter Abbeel, and Sergey Levine. Model-agnostic meta-learning for fast adaptation of deep networks. volume 70 of *Proceedings of Machine Learning Research*, pages 1126–1135, International Convention Centre, Sydney, Australia, 06–11 Aug 2017. PMLR. [2](#), [3](#)
- [6] ZongYuan Ge, Sergey Demyanov, Zetao Chen, and Rahil Garnavi. Generative openmax for multi-class open set classification, 2017. [3](#)
- [7] Spyros Gidaris and Nikos Komodakis. Dynamic few-shot visual learning without forgetting. In *Proceedings of the IEEE Conference on Computer Vision and Pattern Recognition*, pages 4367–4375, 2018. [4](#), [8](#)
- [8] Ian Goodfellow, Jonathon Shlens, and Christian Szegedy. Explaining and harnessing adversarial examples. In *International Conference on Learning Representations*, 2015. [2](#)
- [9] Kaiming He, Xiangyu Zhang, Shaoqing Ren, and Jian Sun. Deep residual learning for image recognition. In *Proceedings of the IEEE conference on computer vision and pattern recognition*, pages 770–778, 2016. [1](#)
- [10] K. He, X. Zhang, S. Ren, and J. Sun. Deep residual learning for image recognition. In *2016 IEEE Conference on Computer Vision and Pattern Recognition (CVPR)*, pages 770–778, 2016. [6](#)
- [11] Dan Hendrycks and Kevin Gimpel. A baseline for detecting misclassified and out-of-distribution examples in neural networks. *Proceedings of International Conference on Learning Representations*, 2017. [1](#), [2](#), [3](#), [5](#)
- [12] Timothy Hospedales, Antreas Antoniou, Paul Micaelli, and Amos Storkey. Meta-learning in neural networks: A survey, 2020. [2](#)
- [13] Alexis Joly and Olivier Buisson. Logo retrieval with a contrario visual query expansion. pages 581–584, 01 2009. [5](#), [11](#)
- [14] Junsik Kim, Tae-Hyun Oh, Seokju Lee, Fei Pan, and In So Kweon. Variational prototyping-encoder: One-shot learning with prototypical images. In *Proceedings of the IEEE Conference on Computer Vision and Pattern Recognition*, pages 9462–9470, 2019. [2](#), [3](#), [4](#), [5](#), [6](#), [7](#), [11](#)
- [15] Diederik P. Kingma and Jimmy Ba. Adam: A method for stochastic optimization, 2017. [6](#)
- [16] Diederik P. Kingma and Max Welling. Auto-Encoding Variational Bayes. In *2nd International Conference on Learning Representations, ICLR 2014, Banff, AB, Canada, April 14-16, 2014, Conference Track Proceedings*, 2014. [3](#), [4](#)
- [17] Pierre Letessier, Olivier Buisson, and Alexis Joly. Scalable mining of small visual objects. 10 2012. [5](#), [11](#)
- [18] Shiyu Liang, Yixuan Li, and R. Srikant. Enhancing the reliability of out-of-distribution image detection in neural networks, 2020. [3](#)
- [19] Tsung-Yi Lin, Piotr Dollár, Ross Girshick, Kaiming He, Bharath Hariharan, and Serge Belongie. Feature pyramid networks for object detection. In *Proceedings of the IEEE conference on computer vision and pattern recognition*, pages 2117–2125, 2017. [1](#)
- [20] B. Liu, H. Kang, H. Li, G. Hua, and N. Vasconcelos. Few-shot open-set recognition using meta-learning. In *2020 IEEE/CVF Conference on Computer Vision and Pattern Recognition (CVPR)*, pages 8795–8804, 2020. [2](#), [3](#), [4](#), [6](#), [7](#), [8](#), [11](#)
- [21] Jinlu Liu, Liang Song, and Yongqiang Qin. Prototype rectification for few-shot learning. *ArXiv*, abs/1911.10713, 2019. [4](#), [8](#)
- [22] Ziwei Liu, Zhongqi Miao, Xiaohang Zhan, Jiayun Wang, Boqing Gong, and Stella X. Yu. Large-scale long-tailed recognition in an open world. In *IEEE Conference on Computer Vision and Pattern Recognition (CVPR)*, 2019. [1](#), [5](#)
- [23] Jonathan Long, Evan Shelhamer, and Trevor Darrell. Fully convolutional networks for semantic segmentation. In *Proceedings of the IEEE conference on computer vision and pattern recognition*, pages 3431–3440, 2015. [1](#)
- [24] Jiajun Lu, Theerasit Issaranon, and David Forsyth. Safetynet: Detecting and rejecting adversarial examples robustly. In *Proceedings of the IEEE International Conference on Computer Vision (ICCV)*, Oct 2017. [1](#)
- [25] Lawrence Neal, Matthew Olson, Xiaoli Fern, Weng-Keen Wong, and Fuxin Li. Open set learning with counterfactual images. In *Proceedings of the European Conference on Computer Vision (ECCV)*, September 2018. [3](#)
- [26] Alex Nichol, Joshua Achiam, and John Schulman. On first-order meta-learning algorithms. *CoRR*, abs/1803.02999, 2018. [3](#)
- [27] Marco A. F. Pimentel, David A. Clifton, Lei Clifton, and Lionel Tarassenko. Review: A review of novelty detection. 99:215–249, June 2014. [2](#), [3](#)
- [28] Dripta S Raychaudhuri and Amit K Roy-Chowdhury. Exploiting temporal coherence for self-supervised one-shot video re-identification. *arXiv preprint arXiv:2007.11064*, 2020. [2](#)
- [29] Marcus Rohrbach, Sandra Ebert, and Bernt Schiele. Transfer learning in a transductive setting. In *Advances in neural information processing systems*, pages 46–54, 2013. [2](#)

- [30] Stefan Romberg, Lluís Pueyo, Rainer Lienhart, and Roelof Zwol. Scalable logo recognition in real-world images. page 25, 01 2011. [5](#), [11](#)
- [31] Nikolay Savinov, Anton Raichuk, Raphaël Marinier, Damien Vincent, Marc Pollefeys, Timothy Lillicrap, and Sylvain Gelly. Episodic curiosity through reachability. In *International Conference on Learning Representations (ICLR)*, 2019. [5](#)
- [32] Jake Snell, Kevin Swersky, and Richard Zemel. Prototypical networks for few-shot learning. In *Proceedings of the 31st International Conference on Neural Information Processing Systems, NIPS'17*, page 4080–4090, Red Hook, NY, USA, 2017. Curran Associates Inc. [2](#), [3](#), [4](#), [6](#), [7](#), [8](#), [11](#)
- [33] Johannes Stalkamp, Marc Schlipf, Jan Salmen, and Christian Igel. Man vs. computer: Benchmarking machine learning algorithms for traffic sign recognition. *Neural networks : the official journal of the International Neural Network Society*, 32:323–32, 02 2012. [5](#), [11](#)
- [34] Hang Su, Xiatian Zhu, and S. Gong. Deep learning logo detection with data expansion by synthesising context. *2017 IEEE Winter Conference on Applications of Computer Vision (WACV)*, pages 530–539, 2017. [5](#), [11](#)
- [35] Hung-Yu Tseng, Hsin-Ying Lee, Jia-Bin Huang, and Ming-Hsuan Yang. Cross-domain few-shot classification via learned feature-wise transformation. *arXiv preprint arXiv:2001.08735*, 2020. [5](#)
- [36] Laurens van der Maaten and Geoffrey Hinton. Visualizing data using t-sne. *Journal of Machine Learning Research*, 9(86):2579–2605, 2008. [8](#)
- [37] Oriol Vinyals, Charles Blundell, Timothy Lillicrap, Koray Kavukcuoglu, and Daan Wierstra. Matching networks for one shot learning. In *Proceedings of the 30th International Conference on Neural Information Processing Systems, NIPS'16*, page 3637–3645, Red Hook, NY, USA, 2016. Curran Associates Inc. [2](#), [3](#), [5](#), [11](#)
- [38] Z. Zhu, D. Liang, S. Zhang, X. Huang, B. Li, and S. Hu. Traffic-sign detection and classification in the wild. In *2016 IEEE Conference on Computer Vision and Pattern Recognition (CVPR)*, pages 2110–2118, 2016. [5](#), [11](#)

Appendix

A. Datasets

In this section we go over the details of each dataset used in our experiments. A summary of the statistics of each dataset is shown in Table 5.

	GTSRB	TT100K	BelgaLogos	Flickr-32	TopLogos	miniImageNet
Number of Samples	51,839	11,988	9,585	3,404	848	60,000
Total Classes	43	36	37	32	11	100

Table 5: Number of samples and classes in each Dataset.

A.1. Traffic Sign Datasets.

GTSRB. This dataset [33] is one of the largest traffic-sign dataset. It is comprised of 43 classes broadly categorized under prohibitory, danger and mandatory categories. For GTSRB→GTSRB, the training set contains a total of 39,209 images and the test set has a total of 12,630 images. These images have variations in illumination, shading as well as, resolution [14].

TT100K. The Tsinghua-Tencent 100K (TT100K) [38] is a Chinese traffic sign detection dataset. This dataset has more than 200 categories, out of which we used the ones with valid annotation and a corresponding exemplar. Similar to [14] this amounts to a total of 36 valid classes to work with.

A.2. Brand Logo Datasets

BelgaLogos. BelgaLogos [13, 17] is comprised of 10,000 images of everyday brand logos commonly found in almost every aspect of daily life. The images have significant perturbations such as blurring, lighting and contrast variations as well as, occlusions. The dataset is also riddled with significant class imbalance as it contains classes with as little as 2 samples making it suitable for only 1-shot learning problems. Similar to [14] we collect 9,475 images from BelgaLogos categorised among 37 logo classes to construct our logo recognition dataset. The images of this dataset have a lot more variations compared to the traffic sign datasets, especially blurring and occlusion, which in-turn makes learning harder.

FlickrLogos-32. This dataset [30] is comprised of a collection of images corresponding to the 32 brand logos of Flickr. We use the splits introduced in [14], which is comprised of a total of 3,372 cropped logo images.

TopLogo-10. This dataset [34] contains logo images from 10 brands related to popular cloth, shoes and accessory brands. The logo images are obtained from their respective products and similar to [14] the collected images were cropped from bounding box annotations and divided among 11 classes where the ‘Adidas’ class is divided into ‘Adidas-logo’ and the ‘Adidas-text’.

A.3. Natural Image Dataset

miniImageNet. Originally proposed by Vinyals et. al. [37], miniImageNet has become a benchmark dataset for few-shot classification [32, 20]. It is derived from the larger ILSVRC-12 dataset [4] and is comprised of 100 classes each having 600 colored images, which are popularly resized to 84×84 [32, 37]. We use the same splits as [37] which comprises of a training set with 64 classes, a validation set with 16 classes and a test set with 20 classes.

B. Sampling Strategies

The episodic sampling strategies for all the experiments performed is shown in Table 6. For an N-way K shot problem each episode has $\mathbf{K}_{Q_{in}}^c$ number of in-distribution queries sampled from each support class $c \in \{1, \dots, N\}$. This means the total number in-distribution query samples per episode $\mathbf{K}_{Q_{in}} = \sum_{c=1}^N \mathbf{K}_{Q_{in}}^c$. Along with the in-distribution samples, the query set of each episode is also augmented with $\mathbf{K}_{Q_{out}}$ samples which do not belong to any of the support classes i.e. out-of-distribution. Hence, the total number samples \mathbf{K}_e , in each episode is given as, $\mathbf{K}_e = \mathbf{K} + \mathbf{K}_{Q_{in}} + \mathbf{K}_{Q_{out}}$ where, $\mathbf{K} = |\mathcal{S}|$. The model encounters \mathbf{E}_{train} number of episodes each epoch during the meta-training phase which means for T epochs the model is trained over a total of $T \times \mathbf{E}_{train}$ number of episodes. Finally, the model is tested over \mathbf{E}_{test} number of test episodes and the average performance is recorded.

DATASETS	GTSRB→GTSRB		GTSRB→TT100K		Belga→Flickr32	Belga→Toplogos	miniImageNet→miniImageNet	
EXPERIMENT	5-way 5-shot	5-way 1-shot	5-way 5-shot	5-way 1-shot	5-way 1-shot	5-way 1-shot	5-way 1-shot	5-way 1-shot
$K_{Q_{in}}^c$	10	10	10	10	1	1	15	15
$K_{Q_{out}}$	50	50	50	50	5	5	75	75
E_{train}	20	20	20	20	50	50	50	50
E_{test}	800	800	800	800	1700	400	600	600

Table 6: Episodic sampling strategy for each of the few-shot experiments.

C. Training Strategy

For the traffic sign and brand logo classification, all modules of ReFOCS are trained end-to-end. However, for *miniImageNet* training the entire framework end-to-end results in over-powering of the reconstruction module resulting in decreased classification accuracy. We suspect, this problem is due to the difficult image-to-exemplar translation task for *miniImageNet* which is brought about by the fact that the exemplars of *miniImageNet* do not lie on a canonical domain, resulting in an embedding space where the seen class clusters have limited separation. In order to rectify this, we first meta-train the classification module i.e. the encoder with just the cross-entropy classification loss (Eq. 6), following the trained encoder is fixed and utilized to jointly train the decoder and the novelty detection module using a combination of the reconstruction loss (Eq. 2) and the novelty detection loss (Eq. 8). This bifurcated training methodology also allows us to explore pre-training of the encoder, which involves normal supervised training of the encoder on the entire base training set. The pre-trained encoder is then meta-trained with the classification loss as explained before. We find that pre-training in general does not give any performance boost for the 5-shot scenario but results in approximately 5% increase in AUROC for the 1-shot case.

D. Implementation Details

Traffic Sign Recognition. For all the traffic sign experiments the images were resized to 64×64 and a learning rate (lr) of 10^{-4} is used. For the GTSRB→GTSRB 5-shot and GTSRB→TT100K 1-shot case, we observe that dropping the lr by a factor of 10 after 13000 and 18000 episodes result in a slight performance increase. The loss function hyperparameters λ_1 , λ_2 and λ_3 , for all the traffic sign experiments, are set to 10^{-4} , 10 and 10 respectively. The temperature parameter τ was initialized with a value of 10 for all the traffic sign experiments.

Brand Logo Recognition. In case of all the 1-shot brand logo experiments the lr is fixed at 10^{-4} . The brand logo images are also resized to 64×64 . For these experiments too, τ is initialized to 10, and the values of λ_1 , λ_2 and λ_3 are set to 10^{-4} , 10 and 10 respectively.

Natural Image Classification. For *miniImageNet* the popular 84×84 image size is used, and for both the 1-shot and 5-shot experiments the lr is initially set to 10^{-3} and then dropped by a factor of 10 after every 20000 episodes. Since, in this case, the encoder is separately meta-trained, the hyperparameter corresponding to the classification loss λ_2 is set to 1 and λ_1 and λ_3 are set to 10^{-4} and 10 respectively. For the 5-shot scenario τ is initialized to a value of 1000, and for the 1-shot case it is initialized to 100.

E. Ablations

More ablation results are shown in tables 7 and 8. The details of each type ablation is provided in Section 4.4. We also show a few sample exemplar reconstructions in Fig 6. As hypothesized when the out-of-distribution query samples are fed into the model it fails to produce any meaningful reconstruction of the class-wise exemplars provided in the support set.

GTSRB→GTSRB				
EXPERIMENT	5-way 5-shot		5-way 1-shot	
	Acc.(%)	AUROC(%)	Acc.(%)	AUROC(%)
Recons. w/ AE	94.11 ± 0.37	94.61 ± 0.32	83.83 ± 0.79	91.81 ± 0.45
No modulation	93.11 ± 0.45	88.67 ± 0.55	84.34 ± 0.75	91.04 ± 0.54
ProtoC+ND	89.72 ± 0.56	82.23 ± 0.79	82.79 ± 0.78	77.56 ± 0.92
No embedding	93.55 ± 0.41	88.80 ± 0.61	85.78 ± 0.72	88.62 ± 0.61
No clf	94.09 ± 0.35	94.03 ± 0.34	84.62 ± 0.78	92.10 ± 0.43
ReFOCS (Ours)	94.17 ± 0.38	94.83 ± 0.35	86.21 ± 0.78	93.02 ± 0.45

GTSRB→TT100K				
EXPERIMENT	5-way 5-shot		5-way 1-shot	
	Acc.(%)	AUROC(%)	Acc.(%)	AUROC(%)
Recons. w/ AE	81.33 ± 0.80	77.08 ± 0.79	68.59 ± 0.88	75.71 ± 0.71
No modulation	80.94 ± 0.79	78.55 ± 0.65	69.84 ± 0.91	77.75 ± 0.54
ProtoC+ND	76.92 ± 0.83	72.50 ± 0.61	68.59 ± 0.83	71.61 ± 0.76
No embedding	83.03 ± 0.75	74.33 ± 0.66	70.77 ± 0.87	59.28 ± 0.79
No clf	82.71 ± 0.74	82.85 ± 0.56	69.14 ± 0.94	74.63 ± 0.61
ReFOCS (Ours)	83.36 ± 0.76	85.25 ± 0.56	71.45 ± 0.87	81.98 ± 0.59

Table 7: **Ablation studies on traffic sign recognition.** Recons. w/ AE refers to swapping the VAE with an Autoencoder (AE); No Modulation denotes turning off embedding modulation; No embedding/clf denote the removal of embedding/softmax scores from the input of the novelty module. ProtoC+ND refers to when we donot use exemplars for the reconstruction and consequently, remove the reconstruction errors from the input of the novelty module.

EXPERIMENT	BELGA→FLICKR32		BELGA→TOPLOGOS	
	5-way 1-shot		5-way 1-shot	
	Acc.(%)	AUROC(%)	Acc.(%)	AUROC(%)
Recons. w/ AE	63.13 ± 1.05	71.86 ± 0.86	36.40 ± 2.00	56.37 ± 1.95
No modulation	63.26 ± 1.03	56.69 ± 0.97	41.75 ± 1.99	52.83 ± 1.93
ProtoC+ND	61.64 ± 1.03	50.01 ± 0.99	41.60 ± 2.04	50.52 ± 2.06
No embedding	65.49 ± 1.00	67.79 ± 0.91	41.45 ± 2.01	53.52 ± 2.11
No clf	64.51 ± 1.01	71.58 ± 0.87	38.60 ± 1.96	56.62 ± 1.86
ReFOCS (Ours)	66.29 ± 1.02	72.98 ± 0.83	42.30 ± 2.15	58.39 ± 1.97

Table 8: **Ablation studies on brand logo recognition.** Recons. w/ AE refers to swapping the VAE with an Autoencoder (AE); No Modulation denotes turning off embedding modulation; No embedding/clf denote the removal of embedding/softmax scores from the input of the novelty module. ProtoC+ND refers to when we donot use exemplars for the reconstruction and consequently, remove the reconstruction errors from the input of the novelty module.



Figure 6: **Sample exemplar reconstructions for GTSRB→GTSRB.** Exemplar reconstructions of a few query samples from 1 episode of a 5-way classification problem. (a) Class-wise exemplars provided in the support set. (b) In-distribution query samples. (c) Out-of-distribution query samples. (d) Reconstructed exemplars from the in-distribution queries. (e) Reconstructed Exemplars from the out-of-distribution queries.